DEUTSCHES ELEKTRONEN – SYNCHROTRON

DESY 92-162
November 1992

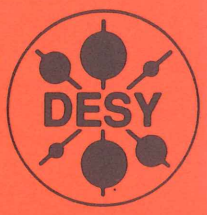

Measurement of the Hadronic Final State in Deep Inelastic Scattering at HERA

H1 Collaboration

ISSN 0418-9833

NOTKESTRASSE 85 · D-2000 HAMBURG 52

To be sure that your preprints are promptly included in the
HIGH ENERGY PHYSICS INDEX,
send them to (if possible by air mail):

DESY
Bibliothek
Notkestraße 85
W-2000 Hamburg 52
Germany

DESY-IfH
Bibliothek
Platanenallee 6
O-1615 Zeuthen
Germany

DESY 92-162
November 1992

ISSN 0418-9833

Measurement of the Hadronic Final State in Deep Inelastic Scattering at HERA

H1 Collaboration

T. Ahmed[3], V. Andreev[22], B. Andrieu[25], M. Arpagaus[32], A. Babaev[21], H. Bärwolff[31], J. Bán[15], P. Baranov[22], E. Barrelet[26], W. Bartel[11], U. Bassler[26], G.A. Beck[17], H.P. Beck[33], H.-J. Behrend[11], A. Belousov[22], Ch. Berger[1], H. Bergstein[1], G. Bernardi[26], R. Bernet[32], U. Berthon[25], G. Bertrand-Coremans[4], M. Besançon[9], P. Biddulph[20], E. Binder[11], J.C. Bizot[24], V. Blobel[13], K. Borras[8], P.C. Bosetti[2], V. Boudry[25], C. Bourdarios[24], F. Brasse[11], U. Braun[2], W. Braunschweig[1], V. Brisson[24], D. Bruncko[15], J. Bürger[11], F.W. Büsser[13], A. Buniatian[11,35], S. Burke[17], G. Buschhorn[23], A.J. Campbell[10], T. Carli[25], F. Charles[26], D. Clarke[5], A.B. Clegg[16], M. Colombo[8], J.A. Coughlan[5], A. Courau[24], Ch. Coutures[9], G. Cozzika[9], L. Criegee[11], J. Cvach[25], J.B. Dainton[17], M. Danilov[21], A.W.E. Dann[20], W.D. Dau[14], M. David[9], E. Deffur[11], B. Delcourt[24], L. DelBuono[26], M. Devel[24], A. DeRoeck[11], P. Dingus[25], C. Dollfus[33], J.D. Dowell[3], H B. Dreis[2], A. Drescher[8], J. Duboc[26], D. Düllmann[13], O. Dünger[13], H. Duhm[12], M. Eberle[12], J. Ebert[30], T.R. Ebert[17], G. Eckerlin[11], V. Efremenko[21], S. Egli[33], S. Eichenberger[33], R. Eichler[32], F. Eisele[11], E. Eisenhandler[18], N.N. Ellis[3], R.J. Ellison[20], E. Elsen[11], M. Erdmann[11], E. Evrard[4], L. Favart[4], A. Fedotov[21], D. Feeken[13], R. Felst[11], J. Feltesse[9], Y. Feng[26], I.F. Fensome[3], J. Ferencei[11], F. Ferrarotto[29], W. Flauger[11,†], M. Fleischer[11], G. Flügge[2], A. Fomenko[22], B. Fominykh[21], M. Forbush[7], J. Formánek[28], J.M. Foster[20], G. Franke[11], E. Fretwurst[12], P. Fuhrmann[1], E. Gabathuler[17], K. Gamerdinger[23], J. Garvey[3], J. Gayler[11], A. Gellrich[13], M. Gennis[11], U. Gensch[31], H. Genzel[1], R. Gerhards[11], D. Gillespie[17], L. Godfrey[7], U. Goerlach[11], L. Goerlich[6], M. Goldberg[26], A.M. Goodall[17], I. Gorelov[21], P. Goritchev[21], C. Grab[32], H. Grässler[2], R. Grässler[2], T. Greenshaw[17], H. Greif[23], G. Grindhammer[23], C. Gruber[14], J. Haack[31], D. Haidt[11], L. Hajduk[6], O. Hamon[26], D. Handschuh[11], E.M. Hanlon[16], M. Hapke[11], J. Harjes[13], P. Hartz[8], R. Haydar[24], W.J. Haynes[5], J. Heatherington[18], V. Hedberg[19], R. Hedgecock[5], G. Heinzelmann[13], R.C.W. Henderson[16], H. Henschel[31], R. Herma[1], I. Herynek[27], W. Hildesheim[26], P. Hill[11], C.D. Hilton[20], J. Hladký[27], K.C. Hoeger[20], Ph. Huet[4], H. Hufnagel[8], N. Huot[26], M. Ibbotson[20], M.A. Jabiol[9], A. Jacholkowska[24], C. Jacobsson[19], M. Jaffre[24], L. Jönsson[19], K. Johannsen[13], D.P. Johnson[4], L. Johnson[16], H. Jung[2], P.I.P. Kalmus[18], S. Kasarian[11], R. Kaschowitz[2], P. Kasselmann[12], U. Kathage[14], H. H.Kaufmann[31], I.R. Kenyon[3], S. Kermiche[24], C. Kiesling[23], M. Klein[31], C. Kleinwort[13], G. Knies[11], T. Köhler[1], H. Kolanoski[8], F. Kole[7], S.D. Kolya[20], V. Korbel[11], M. Korn[8], P. Kostka[31], S.K. Kotelnikov[22], M.W. Krasny[6,9], H. Krehbiel[11], D. Krücker[2], U. Krüger[11], J.P. Kubenka[23], H. Küster[11], M. Kuhlen[23], T. Kurča[15], J. Kurzhöfer[8], B. Kuznik[30], R. Lander[7], M.P.J. Landon[18], R. Langkau[12], P. Lanius[23], J.F. Laporte[9], A. Lebedev[22], A. Leuschner[11], C. Leverenz[11], D. Levin[11], S. Levonian[11,22], Ch. Ley[2], A. Lindner[8], G. Lindström[12], P. Loch[11], H. Lohmander[19], G.C. Lopez[18], D. Lüers[23,†], N. Magnussen[30], E. Malinovski[22], S. Mani[7], P. Marage[4], J. Marks[10], R. Marshall[20], J. Martens[30], R. Martin[17], H.-U. Martyn[1], J. Martyniak[6], S. Masson[2], A. Mavroidis[18],

S.J. Maxfield[17], S.J. McMahon[17], A. Mehta[20], K. Meier[11], T. Merz[11], C.A. Meyer[33], H. Meyer[30], J. Meyer[11], S. Mikocki[6,24], V. Milone[29], E. Monnier[26], F. Moreau[25], J. Moreels[4], J.V. Morris[5], J.M. Morton[17], K. Müller[33], P. Murín[15], S.A. Murray[20], V. Nagovizin[21], B. Naroska[13], Th. Naumann[31], D. Newton[16], H.K. Nguyen[26], F. Niebergall[13], R. Nisius[1], G. Nowak[6], G.W. Noyes[3], M. Nyberg[19], H. Oberlack[23], U. Obrock[8], J.E. Olsson[11], S. Orenstein[25], F. Ould-Saada[13], C. Pascaud[24], G.D. Patel[17], E. Peppel[11], S. Peters[23], H.T. Phillips[3], J.P. Phillips[20], Ch. Pichler[12], W. Pilgram[2], D. Pitzl[32], R. Prosi[11], F. Raupach[1], K. Rauschnabel[8], P. Reimer[27], P. Ribarics[23], V. Riech[12], J. Riedlberger[32], M. Rietz[2], S.M. Robertson[3], P. Robmann[33], R. Roosen[4], A. Rostovtsev[21], C. Royon[9], M. Rudowicz[23], M. Ruffer[12], S. Rusakov[22], K. Rybicki[6], E. Ryseck[31], J. Sacton[4], N. Sahlmann[2], E. Sanchez[23], D.P.C. Sankey[5], M. Savitsky[11], P. Schacht[23], P. Schleper[1], W. von Schlippe[18], C. Schmidt[11], D. Schmidt[30], W. Schmitz[2], V. Schröder[11], M. Schulz[11], A. Schwind[31], W. Scobel[12], U. Seehausen[13], R. Sell[11], M. Seman[15], A. Semenov[21], V. Shekelyan[21], I. Sheviakov[22], H. Shooshtari[29], G. Siegmon[14], U. Siewert[14], Y. Sirois[25], I.O. Skillicorn[10], P. Smirnov[22], J.R. Smith[7], L. Smolik[11], Y. Soloviev[22], H. Spitzer[13], P. Staroba[27], M. Steenbock[13], P. Steffen[11], R. Steinberg[2], H. Steiner[26], B. Stella[29], K. Stephens[20], J. Stier[11], J. Strachota[11], U. Straumann[33], W. Struczinski[2], J.P. Sutton[20], R.E. Taylor[34,24], G. Thompson[18], R.J. Thompson[20], I. Tichomirov[21], C. Trenkel[14], P. Truöl[33], V. Tchernyshov[21], J. Turnau[6], J. Tutas[1], L. Urban[23], A. Usik[22], S. Valkar[28], A. Valkarova[28], C. Vallee[26], P. VanEsch[4], A. Vartapetian[11,35], Y. Vazdik[22], M. Vecko[27], P. Verrecchia[9], R. Vick[13], G. Villet[9], E. Vogel[1], K. Wacker[8], I.W. Walker[16], A. Walther[8], G. Weber[13], D. Wegener[8], A. Wegner[11], H. P.Wellisch[23], S. Willard[7], M. Winde[31], G.-G. Winter[11], Th. Wolff[32], L.A. Womersley[17], A.E. Wright[20], N. Wulff[11], T.P. Yiou[26], J. Žáček[24,28], P. Závada[27], C. Zeitnitz[12], H. Ziaeepour[24], M. Zimmer[11], W. Zimmermann[11], and F. Zomer[24]

[1] *I. Physikalisches Institut der RWTH, Aachen, Germany*[a]
[2] *III. Physikalisches Institut der RWTH, Aachen, Germany*[a]
[3] *School of Physics and Space Research, University of Birmingham, Birmingham, UK*[b]
[4] *Inter-University Institute for High Energies ULB-VUB, Brussels, Belgium*[c]
[5] *Rutherford Appleton Laboratory, Chilton, Didcot, UK*[b]
[6] *Institute for Nuclear Physics, Cracow, Poland*
[7] *Physics Department and IIRPA, University of California, Davis, California, USA*[d]
[8] *Institut für Physik, Universität Dortmund, Dortmund, Germany*[a]
[9] *DAPNIA, Centre d'Etudes de Saclay, Gif-sur-Yvette, France*
[10] *Department of Physics and Astronomy, University of Glasgow, Glasgow, UK*[b]
[11] *DESY, Hamburg, Germany*[a]
[12] *I. Institut für Experimentalphysik, Universität Hamburg, Hamburg, Germany*[a]
[13] *II. Institut für Experimentalphysik, Universität Hamburg, Hamburg, Germany*[a]
[14] *Institut für Reine und Angewandte Kernphysik, Universität Kiel, Kiel, Germany*[a]
[15] *Institute of Experimental Physics, Slovak Academy of Sciences, Kosice, CSFR*
[16] *School of Physics and Materials, University of Lancaster, Lancaster, UK*[b]
[17] *Department of Physics, University of Liverpool, Liverpool, UK*[b]
[18] *Queen Mary and Westfield College, London, UK*[b]
[19] *Physics Department, University of Lund, Lund, Sweden*[e]
[20] *Physics Department, University of Manchester, Manchester, UK*[b]

[21] *Institute for Theoretical and Experimental Physics, Moscow, Russia*
[22] *Lebedev Physical Institute, Moscow, Russia*
[23] *Max-Planck-Institut für Physik, München, Germany*[a]
[24] *LAL, Université de Paris-Sud, IN2P3-CNRS, Orsay, France*
[25] *LPNHE, Ecole Polytechnique, IN2P3-CNRS, Palaiseau, France*
[26] *LPNHE, Universités Paris VI and VII, IN2P3-CNRS, Paris, France*
[27] *Institute of Physics, Czechoslovak Academy of Sciences, Praha, CSFR*
[28] *Nuclear Center, Charles University, Praha, CSFR*
[29] *INFN Roma and Dipartimento di Fisica, Universita "La Sapienzia", Roma, Italy*
[30] *Fachbereich Physik, Bergische Universität Gesamthochschule Wuppertal, Wuppertal, Germany*[a]
[31] *DESY, Institut für Hochenergiephysik, Zeuthen, Germany*[a]
[32] *Institut für Mittelenergiephysik, ETH, Zürich, Switzerland*[f]
[33] *Physik-Institut der Universität Zürich, Zürich, Switzerland*[f]
[34] *Stanford Linear Accelerator Center, Stanford California, USA*
[35] *Visitor from Yerevan Phys.Inst., Armenia*
[†] *Deceased*

[a] *Supported by the Bundesministerium für Forschung und Technologie, FRG*
[b] *Supported by the UK Science and Engineering Research Council*
[c] *Supported by IISN-IIKW, NATO CRG-890478*
[d] *Supported in part by USDOE grant DE F603 91ER40674*
[e] *Supported by the Swedish Natural Science Research Council*
[f] *Supported by the Swiss National Science Foundation*

Abstract

We report on the first experimental study of the hadronic final state in deep inelastic electron-proton scattering with the H1 detector at HERA. Energy flow and transverse momentum characteristics are measured and presented both in the laboratory and in the hadronic center of mass frames. Comparison is made with QCD models distinguished by their different treatment of parton emission.

1 Introduction

Since May 1992 when the first electron-proton (ep) collisions were observed at the HERA storage ring, a new kinematic domain of ep physics has become accessible experimentally. In this paper we report on first results of an analysis of the hadronic final state in deep inelastic scattering (DIS) of 26.7 GeV electrons and 820 GeV protons. The data were collected in July 1992 and amount to an integrated luminosity of about 1.6 nb^{-1}.

It is already well established from analyses of previous lower energy lepton-nucleon DIS measurements [1,2,3] that an understanding of the topological characteristics of hadron production requires QCD corrections to the naive quark-parton model. In particular, the observed event shapes and the transverse momentum (p_T) distributions of final state hadrons were described in terms of $O(\alpha_s)$ QCD matrix elements, additional effects of soft gluons, and fragmentation [4].

In the present rather small sample of data, the bulk of events are at momentum transfers Q^2 that have already been observed in previous experiments. However, because the average invariant mass W of the hadronic final state is about 100 GeV, roughly 5 times greater than in the previous experiments, the data presented here are in a new DIS kinematic domain, namely Bjorken x down to 10^{-4}. In the H1 detector we observe the scattered electron and the current jet, as can be seen in the event displayed in fig. 1a) and b), while the fragments from the proton remnants and from initial parton radiation tend to remain inside the beam pipe. Therefore we are sensitive mainly to gluon emission associated with the current quark and to large p_T quark pair production in photon gluon fusion.

We compare our data in terms of hadronic energy flow and p_T both in the laboratory and hadronic center of mass systems with several QCD models which differ in their treatment of parton radiation processes.

2 Detector description

We describe here briefly only the components of the H1 detector used in this analysis (see fig. 1a), referring to [5] for details.

The interaction region is surrounded by the central tracker (CT). It consists of two cylindrical "jet" drift chambers for charged track reconstruction in the plane transverse to the beam interleaved with "z" drift chambers to improve track polar angle (θ)

measurement. The uniform 1.2 T field is provided in the CT region by a large superconducting solenoidal magnet which surrounds the trackers and the central calorimeter. In the "backward" direction (the electron beam and $-z$ direction) the backward multiwire proportional chamber (BPC) measures the polar angle θ_e of the scattered electron and is used in the scattered electron identification and kinematic reconstruction.

Outside the track detectors are calorimeters for electromagnetic and hadronic energy measurement. A finely segmented liquid argon (LAr) calorimeter covers the forward (the proton beam and $+z$ direction) and central regions ($4^0 < \theta < 155^0$). It consists of an electromagnetic section (EMC) of between 20 and 30 radiation lengths (X_0) depth followed by an hadronic section (HAC). The total depth of the LAr calorimeter varies between 4.5 and 8 interaction lengths.

The initial calibration of the LAr calorimeter was achieved with test beam measurements using electrons and pions at CERN. The absolute scale of the energy response at HERA has been verified with charged particles by comparing their momentum measured in the CT with associated energy deposited in the calorimeter. With electrons and positrons produced by cosmic ray muons, the electromagnetic scale has been checked to $\pm 2\%$ [6]. Using negatively charged particle tracks originating from the ep interaction region, the hadronic scale has been checked to $\pm 10\%$. Furthermore, a study of the balance of transverse momentum between the scattered electron measured in the backward calorimeter and the recoiling hadronic system measured in the LAr calorimeter has so far verified that the overall hadronic energy scale of the LAr calorimeter is understood to within $\pm 7\%$.

The backward region ($154^0 \lesssim \theta < 176^0$) is covered by a 22 X_0 deep lead-scintillator electromagnetic calorimeter (BEMC). The overall calibration of the BEMC calorimeter to $\pm 2\%$ was achieved by using kinematic constraints in DIS events [7]. A hodoscope consisting of 2 planes of scintillators (TOF) is placed behind the BEMC. It provides time-of-flight information to reject out of time proton beam background originating upstream.

A luminosity detector which measures the reaction $ep \rightarrow e\gamma p$ is placed in the backward direction with components at $z = -33$ m to tag electrons scattered at small angles and at $z = -103$ m to measure photons.

3 Event Selection

For this analysis only a subsample of our DIS candidate events is used in which the electron is scattered into the BEMC calorimeter and substantial hadronic energy deposition is observed in the detector.

The hardware trigger requires an energy cluster with more than 4 GeV deposited in the BEMC and no time of flight veto from the scintillator hodoscope. The trigger efficiency is $> 99\%$ for the final sample of selected events because an energetic BEMC cluster is required [7]. After reconstruction, the data are subjected to the following selection criteria:

1. the scattered electron, defined as the most energetic BEMC cluster, must have energy greater than 14 GeV and be associated within 15 cm with a hit in the BPC; to ensure a precise energy measurement, the cluster center of gravity (c.o.g.) must not be too close to the beam pipe, i.e. $|x_{\mathrm{c.o.g}}| > 16$ cm or $|y_{\mathrm{c.o.g}}| > 16$ cm;

2. the BPC hit must lie between 18 and 60 cm from the beam line, i.e. the electron scattering angle is between 173° and 157° when the collision occurs at the nominal ep interaction point;

3. the invariant mass squared W^2 of the hadronic system must be greater than 3000 GeV^2;

4. the event vertex, determined from central charged tracks, must lie within ± 50 cm of the nominal ep interaction point (the event vertex distribution is spread in z with a FWHM of 40 cm due to the length of the proton bunches in HERA);

Selection 1 eliminates the background from photoproduction in which an energetic π^0 fakes a DIS electron [7]. Selection 2 ensures good containment of the electron shower in the BEMC. Selection 3 ensures substantial hadronic energy flow into the H1 detector. Selection 4 ensures that a meaningful determination of kinematic variables is possible. Fig. 1c shows the distribution in x and Q^2 for the final sample of 88 events after visual identification and rejection of 6 remaining background events (p-gas or p-beam wall interaction).

For the hadron analysis only tracks other than the electron which meet the following requirements are used:

- they must be measured in the central tracking chamber with at least 10 hits (out of a maximum of 56) and have a polar angle between 22° and 160°;

- after being constrained to the average beam position in the transverse plane, they must have a transverse momentum p_T of more than 100 MeV and a fractional momentum error $\sigma(p)/p$ of less than 0.5.

The reconstruction efficiency for tracks fulfilling these conditions in our DIS sample is $95 \pm 2\%$ obtained from the visual scan.

For the calorimetric measurement of the hadronic energy flow we use the cells of the liquid argon and BEMC calorimeters. Electronic noise is included in the detector simulation using H1 events recorded with random triggers. After off-line reconstruction, the summed contribution of the electronic noise in all LAr calorimeter cells to the energy measurement is 0.3 GeV with an $r.m.s.$ of 0.9 GeV.

4 Kinematics of the DIS Events

In DIS events, kinematic variables can be determined from either the scattered electron or the produced hadrons. A comparison of the two is a good check that the data satisfy the kinematic constraints of energy and momentum conservation. Such a check is most

effectively carried out by comparing estimates of both the momentum transverse to the beam axis p_T and the DIS scaling variable y.

Both p_T and y are determined from the energy E'_e and polar angle θ_e of the scattered electron using the expressions

$$p_{Te} = E'_e \sin\theta_e \qquad\qquad y_e = 1 - \frac{E'_e}{E_e}\sin^2\frac{\theta_e}{2}$$

where E_e is the incident electron energy taken to be the beam energy.

For the measurement of y from the hadronic system we use the Jacquet-Blondel method [8], namely

$$y_h = \sum_{hadrons} \frac{E_h - p_{zh}}{2E_e},$$

where E_h is the energy of a hadron and p_{zh} its momentum component along the $+z$ direction. y_h can be determined either by summing over all calorimeter cells or over a combination of tracks and calorimeter cells. Since in our data sample most of the events are at low Q^2 with correspondingly low particle energies and multiplicities, we find that the combined method is more precise, and so we use it for the determination of y_h.

The electron/hadron comparison of p_T and y can be summarized by examining the means and widths of the distributions of the ratios p_{Th}/p_{Te} and y_h/y_e.

	$< p_{Th}/p_{Te} >$	*r.m.s.*	$< y_h/y_e >$	*r.m.s.*
data	0.83 ± 0.04	0.34	0.86 ± 0.04	0.31
MC	0.86 ± 0.01	0.34	0.87 ± 0.01	0.34

For the comparison of transverse momenta a cut in the electron transverse momentum of $p_{Te} > 3$ GeV is applied. p_{Th} is the negative transverse component of the hadronic momentum vector projected onto the electron direction and is measured with calorimeter energies. The ratio y_h/y_e is studied here for a subsample of events satisfying $y_e > 0.1$ to allow a good determination of y_e. The data are compared with a detailed simulation of DIS events after the same selection criteria have been applied. With our present statistics, the reconstruction of kinematics is not sensitive to the QCD model used. We conclude from these comparisons that the selected sample of DIS events is consistent with kinematic expectation. The discrepancies of the mean values of the ratios quoted above from unity are expected because, for the low Q^2 of these data, the hadronic energies are low and sometimes not visible in the LAr calorimeter. These discrepancies are however well reproduced by MC simulation demonstrating that the measurement of tracks and calorimetric energy flow in this kinematic region is well understood.

In the following, we will use the scaling variable x and the hadronic invariant mass W determined using

$$x = \frac{Q^2}{sy_h} \qquad\qquad W^2 = sy_h - Q^2 + M^2$$

where s is the ep center of mass energy (87600 GeV^2), M is the proton mass and Q^2 is obtained from the electron with

$$Q^2 = 4E'_e E_e \cos^2\frac{\theta_e}{2}\,.$$

The Lorentz transformation from the laboratory system to the hadronic center of mass (CMS) is performed using y_h and the direction and energy of the scattered electron, since this combination is relatively insensitive to QED radiation effects.

5 QCD Models and Simulation

In the comparison of our data with theoretical models, we investigate three different prescriptions for the simulation of QCD effects in deep inelastic scattering. We restrict ourselves to one model for soft parton fragmentation, namely the Lund string model as implemented in JETSET [9], and to a parametrization of the proton structure function (MRSD0 [10]) which describes data [11] at values of $x > 8 \cdot 10^{-3}$ and is consistent with our data at lower values of x [7]. The QCD prescriptions are as follows.

Leading log parton showers (PS)
In ep collisions two parton cascades are generated, one from the time-like scattered parton, and one from the space-like initial parton in the proton. The amount and hardness of the gluon radiation depend sensitively on the virtuality of the parton before and after the quark-photon vertex. In ep scattering Q^2 or W^2 or some function of both can be chosen as the scale for the maximum of the allowed virtuality. In this experiment we investigate for the first time the kinematic region where $< Q^2 > \approx 15$ GeV^2 and $< W^2 > \approx 10^4$ GeV^2, in which significantly more gluon radiation is predicted using the higher W^2 scale. For comparison with data, we have chosen the two scales Q^2 and W^2. Distributions for each of these two cases we denote with PS(Q^2) and PS(W^2). The corresponding events have been generated using HERACLES 3.1 [12] for the electroweak interaction, including first order radiative corrections, followed by LEPTO 5.2 [13] for the simulation of QCD processes.

Color dipole model (CDM)
In contrast to the bremsstrahlung-like parton shower model, the CDM does not distinguish between initial and final state radiation. It assumes that gluon emission can be described by a chain of radiating color dipoles starting with a dipole formed between the scattered point-like quark and the extended proton remnant. In this model as implemented in ARIADNE [15], the scale is given by the p_T^2 of the radiated gluon and its maximum is proportional to $W^{4/3}$. Distributions labelled with CDM are based on events generated with LEPTO 6.1 [14] for the electroweak interaction and photon-gluon fusion in first order QCD, followed by ARIADNE 4.03 for parton emission in CDM.

$O(\alpha_s)$ matrix element and parton showers (ME+PS)
Here the photon gluon fusion and gluon radiation processes are simulated using exact order α_s matrix elements, and additional softer emissions are added using the parton shower model. In the approach adopted in LEPTO 6.1 [14] the maximum virtuality scale is related to the first order matrix element. Distributions generated with this program are labelled with ME+PS.

The implementations of CDM and ME+PS do not include QED radiative corrections. The requirement of $E'_e > 14$ GeV for the scattered electron implies $y_e \lesssim 0.5$. Therefore the radiative corrections are small ($< 5\%$) for the distributions which we discuss below. This has been verified using HERACLES. The effect of choosing MRSD$-$, a different parametrization of the structure function which in our kinematic region has a more steeply falling x dependence ($\propto 1/\sqrt{x}$), gives rise to changes in some of the distributions of typically less than 15%. Both effects however have no impact on our conclusions.

The results of the event generation are fed into the H1 detector simulation program, which is based on the GEANT package [16] and contains a precise description of the H1 geometry. The calorimetric response of this program has been extensively compared and tuned to test-beam results [17]. The resulting simulated events are subject to the same reconstruction and analysis chain as the real data.

6 Results

The distributions shown are not corrected for detector acceptance and resolution. They are compared with model calculations including a full simulation of the H1 detector. The detector effects are small because the simulated distributions differ by less than 20% from the generated ones[1]. It is important to note that in all subsequent figures each event contributes to more than one data point, and therefore that there exist correlations between data points.

In a study of experimental systematic effects the criteria for event and track selection as well as the details of the calorimetric energy reconstruction and noise suppression scheme have been varied within reasonable bounds. A possible degradation of the track momentum resolution by 10% and the calibration uncertainty of the BEMC ($\pm 2\%$ to date) have a negligible influence on the results. The biggest source of systematic error is the absolute hadronic calibration of the liquid argon calorimeter ($\pm 7\%$ uncertainty to date), which enters linearly in all calorimetric energy flow measurements. All these systematic effects are small when compared with the differences between the models which our statistical sensitivity allows us to distinguish. As a further check, all calorimetric measurements are confirmed when tracks in the central tracker only are used, though with larger error and over a smaller rapidity range.

Within the chosen acceptance cuts of the central tracker ($22° < \theta < 160°, p_T > 0.1$ GeV) we observe on average about four charged particles per event. Their distribution in transverse momentum p_T with respect to the beam axis falls steeply (fig. 2). The flow of energy measured in the calorimeter transverse to the beam axis, E_T, is shown in fig. 3a as a function of pseudorapidity $\eta = -\ln \tan \frac{\theta}{2}$. Here θ is the polar angle of the energy deposition with respect to the proton beam axis. Fig. 3b shows the flow of E_T, measured with the calorimeter in the rapidity interval $-3 < \eta < 3$, as a function of ϕ. Here ϕ is the angle in the plane transverse to the beam direction between the scattered electron and the energy deposition. We observe the current jet as collimated energy flow balancing the p_T of the electron at $\phi = \pi$.

The most natural frame to study the hadronic final state is its center of mass system (CMS). In this frame we define the z^* axis[2] as the direction of the exchanged virtual photon. In the naive quark parton model the current and target jet fragmentation regions then correspond to the $+z^*$ and $-z^*$ hemispheres. In fig. 4 the energy flow measured with the calorimeter as a function of θ^* is shown, where θ^* is the angle with respect to the $+z^*$ direction. A well collimated current jet is evident. In the

[1] This is not so for calorimetric measurements in the forward region (rapidity > 2) where the difference increases to 50% because particles at small polar angles hit the beam pipe and spray energy into the forward calorimeters.

[2] The transformed variables are denoted with a * as superscript.

hadronic CMS the distribution of particle momenta transverse to the virtual photon direction as function of Feynman x, $x_F = p_z^*/p_z^{*\max}$ is particularly sensitive to different QCD models [2]. Here $p_z^{*\max} = W/2$ is the maximum of the kinematically allowed longitudinal momentum carried by a single particle. Fig. 5 displays the x_F distribution and the mean transverse momentum squared $< p_T^{*2} >$ of the charged particles as a function of x_F ("seagull" plot). We are not sensitive to negative x_F because of the polar angle cut used in this analysis.

In all the above distributions both the ME+PS and the CDM models are in good agreement with the data, and are indistinguishable with the available statistical precision. Both the distributions of transverse energy (figs. 3a, b) and the width of the current jet (figs. 3b, 4, 5) are described correctly. However the parton shower evolution with the large scale, PS(W^2), predicts too much transverse energy, and the evolution with the small scale, PS(Q^2), predicts too little (figs. 3,4). The same effect is seen in the "seagull" plot (fig. 5), where PS(W^2) is found to overestimate the average p_T^{*2} of the produced particles while PS(Q^2) underestimates it. Varying Λ_{QCD} between 10 and 800 MeV for PS(Q^2) and PS(W^2) does not lead to an adequate description of our data. The prediction of the simple quark parton model without QCD corrections is found to be similar to the PS(Q^2) model and can thus also be excluded. This is true even if we increase the parameter governing the p_T generated in the fragmentation process by a factor of 2.

Conclusions

The hadronic final state in deep inelastic ep scattering has been measured for the first time at HERA in a new kinematic domain. The data are in good agreement with QCD expectations. The observed widening of the current jet is described when including parton emission. The models based on first order matrix element calculations with additional parton shower evolution and on color dipole radiation are both able to reproduce the data at the present level of statistical sensitivity without any adjustment of parameters from values which describe parton processes in lower energy DIS data. The leading log parton shower approach fails if either W^2 or Q^2 is chosen as the scale governing the amount and hardness of gluon radiation, although an intermediate scale may still be compatible with our data. Forthcoming, more precise data, will allow more stringent comparison as well as other QCD tests.

Acknowledgements

We are grateful to the HERA machine group whose outstanding efforts made this experiment possible. We acknowledge the support of the DESY computer center. We appreciate the imense effort of the engineers and technicians who constructed and maintain the detector. We thank all funding agencies for financial support. The non-DESY members of the collaboration also wish to thank the DESY directorate for the hospitality extended to them. Finally we would like to thank G. Ingelman and L. Lönnblad for illuminating discussions.

References

[1] EMC, J.J. Aubert et al., Phys. Lett. 95B (1980) 306, Phys. Lett.100B (1981) 433, Phys. Lett.119B (1982) 233.

[2] EMC, M. Arneodo et al., Z. Phys. C 36 (1987) 527.

[3] E665 Collab., M.R. Adams et al. Phys. Rev. Lett. 69 (1992) 1026.

[4] Bo Andersson et al. Z. Phys. C 9 (1981) 233,
G. Ingelman et al. Nucl. Phys. B206 (1982) 239.

[5] F. Brasse, to be published in the Proceedings of the 26th International Conference on High Energy Physics, Dallas, 1992 and DESY preprint 92-140(1992);
G. Cozzika, to be published in the Proceedings of the 3rd Int. Conf. on Calorimetry in High Energy Physics, Corpus Christi, 1992.

[6] J. Gayler, to be published in the Proceedings of the 3rd Int. Conf. on Calorimetry in High Energy Physics, Corpus Christi, 1992.

[7] H1 Collab., T.Ahmed et al., "Observation of Deep Inelastic Scattering at Low x", submitted to Physics Letters.

[8] A. Blondel and F. Jacquet, Proceedings of the Study of an *ep* Facility for Europe, ed. U. Amaldi, DESY 79/48 (1979) 391.

[9] T. Sjöstrand, Comp. Phys. Commun. 39 (1986) 347;
T. Sjöstrand and M. Bengtsson, Comp. Phys. Commun. 43 (1987) 367, and for JETSET 7.3, CERN-TH. 6488/92 (1992).

[10] A.D. Martin, W.J. Stirling, R.G. Roberts, Durham preprint, DTP-92-16(1992);
H. Plothow-Besch, Proc. of the 3rd Workshop on Detector and Event Simulation in High Energy Physics, eds. K. Bos and B. van Eijk (NIKHEF-H, Amsterdam, 1991), p. 148 and CERN-PPE 1992.07.22.

[11] NMC Collab., P.Amaudruz et al., CERN PPE-92-124, to appear in Phys.Lett.B.

[12] A. Kwiatkowski, H. Spiesberger, and H.-J. Möhring, Comp. Phys. Commun. 69(1992) 155, and references therein.

[13] G. Ingelman, "LEPTO 5.2", unpublished program manual, see also
H.Bengtsson, G.Ingelman, and T.Sjöstrand, Nucl. Phys. B301 (1988) 554.

[14] G. Ingelman, "LEPTO 6.1", Proc. of the Workshop on Physics at HERA, eds. W. Buchmüller and G. Ingelman, Hamburg, 1991, vol. 3, 1366, and references therein.

[15] L. Lönnblad, ARIADNE version 4.03, Comp. Phys. Commun. 71 (1992) 15, and references therein.

[16] GEANT program manual, CERN program library (1992).

[17] M. Kuhlen, to be published in the Proceedings of the 26th International Conference on High Energy Physics, Dallas, 1992.

Figure 1:
A deep inelastic scattering event in the H1 detector: shown are a) side view of calorimeters (EMC,HAC,BEMC), forward (FT) and central (CT) trackers, backward proportional chamber (BPC), and scintillator hodoscope (TOF), and b) energy flow as measured in the calorimeters as a function of pseudorapidity η and azimuthal angle ϕ. c) shows the distribution of the event sample in the x, Q^2 plane. The arrow points to the event shown in a) and b). Contours of $\theta_e = 157°, 173°$ and of constant y corresponding to $W^2 \approx 3000$ GeV^2, $E'_e \approx 14$ GeV and the kinematic limit ($y = 1$) are indicated.

Figure 2:
Transverse momentum p_T distribution for charged particles with respect to the beam axis in the laboratory frame. Superimposed are the expectations of the different QCD based models. The distribution is normalized to the number of events N, and n refers to the number of tracks.

Figure 3:
Transverse energy flow E_T in the laboratory frame measured with the calorimeter a) as a function of pseudorapidity η; b) as a function of azimuthal angle ϕ with respect to the scattered electron direction in the plane transverse to the beam direction The predictions of the different models are also given.

Figure 4:
Calorimetric energy flow as a function of angle θ^* with respect to the virtual boson direction in the hadronic CMS. The predictions of the various models are superimposed.

Figure 5:
a) Feynman x, x_F, distribution and b) average p_T^{*2} as a function of x_F ("seagull" plot) for charged particles in the hadronic CMS. The model predictions are also shown.

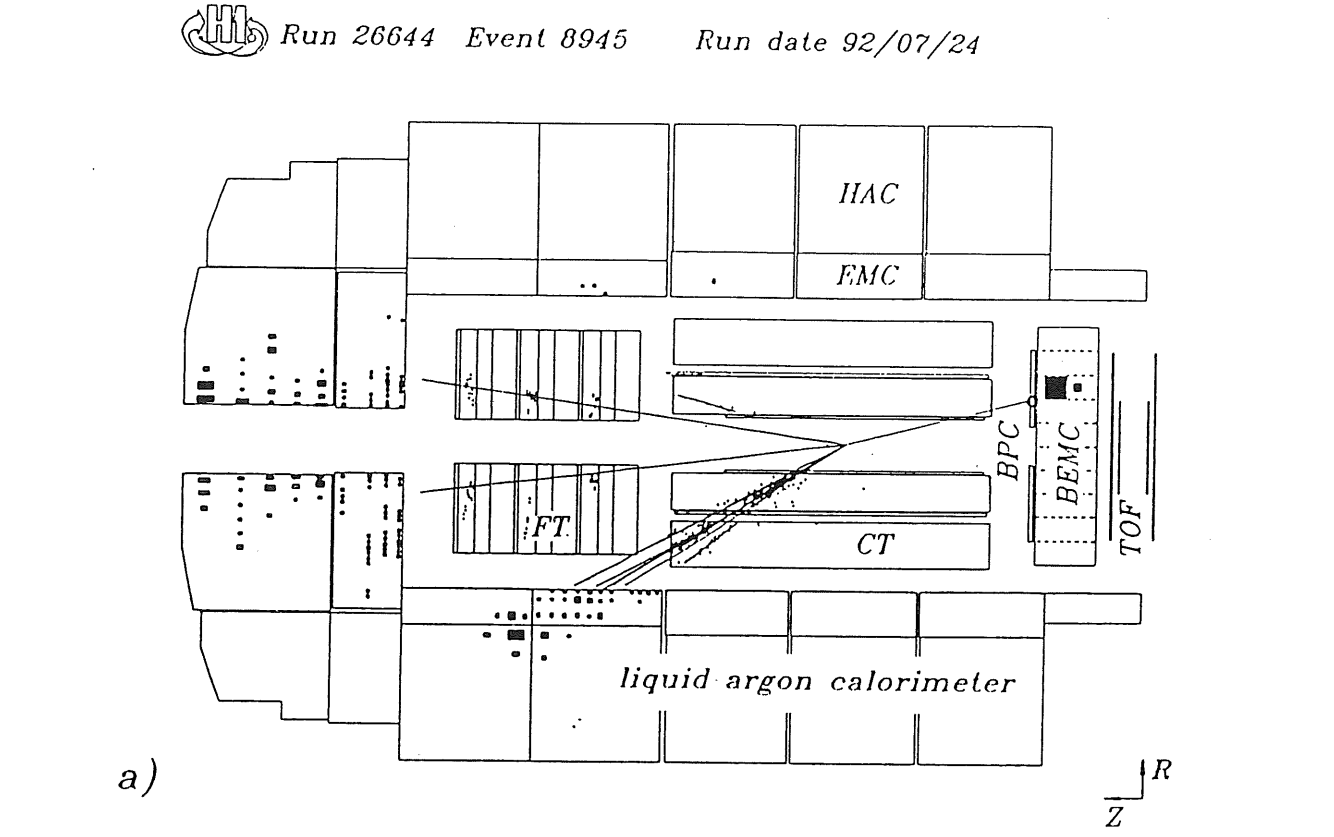
Run 26644 Event 8945 Run date 92/07/24
HAC
EMC
BPC
BEMC
TOF
FT
CT
liquid argon calorimeter
a)
R
Z

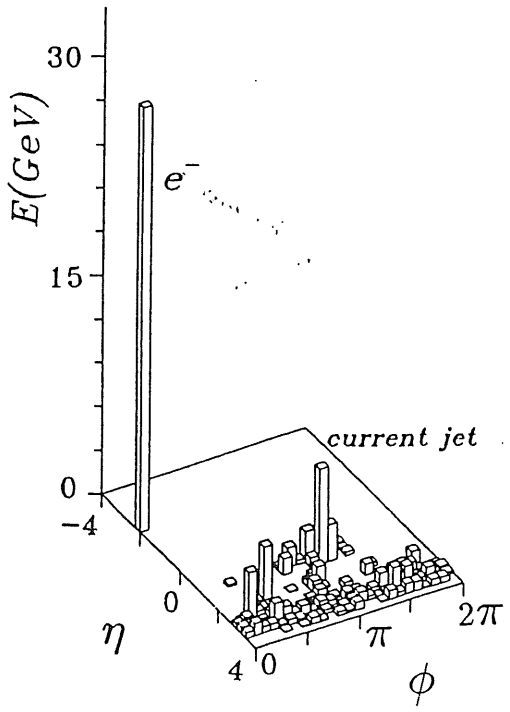
30
15
0
E(GeV)
e⁻
current jet
−4
0
η
4
0
π
2π
φ
b)

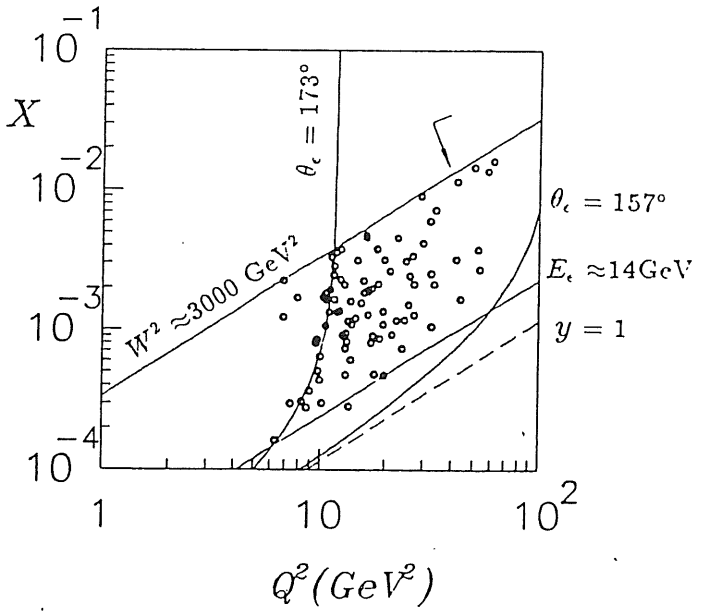
10⁻¹
10⁻²
10⁻³
10⁻⁴
X
θe = 173°
W² ≈3000 GeV²
θe = 157°
Ee ≈14GeV
y = 1
1
10
10²
Q²(GeV²)
c)

Fig. 1

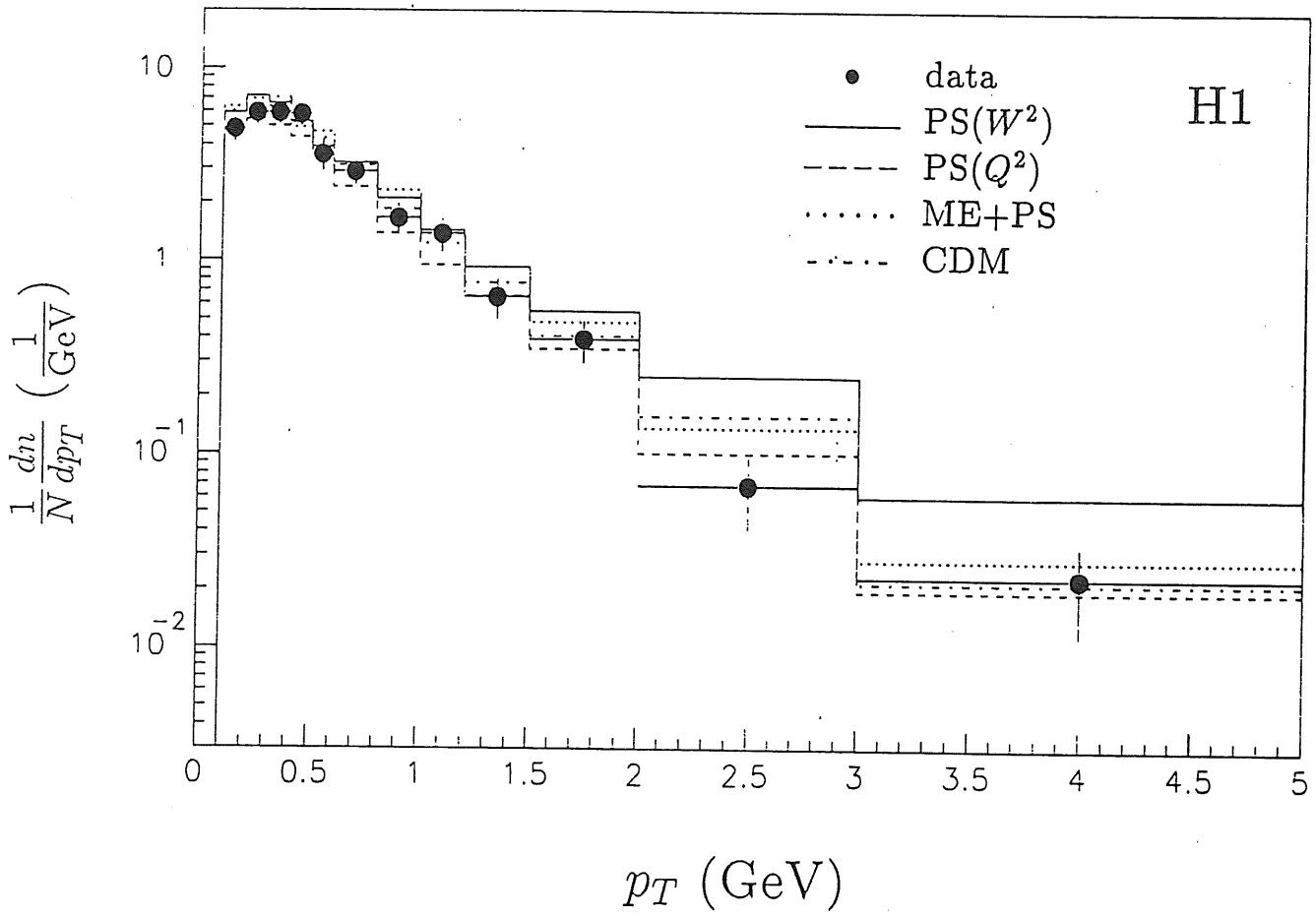
data
PS(W^2)
PS(Q^2)
ME+PS
CDM
H1
$\frac{1}{N}\frac{dn}{dp_T}\left(\frac{1}{\mathrm{GeV}}\right)$
p_T (GeV)

Fig. 2

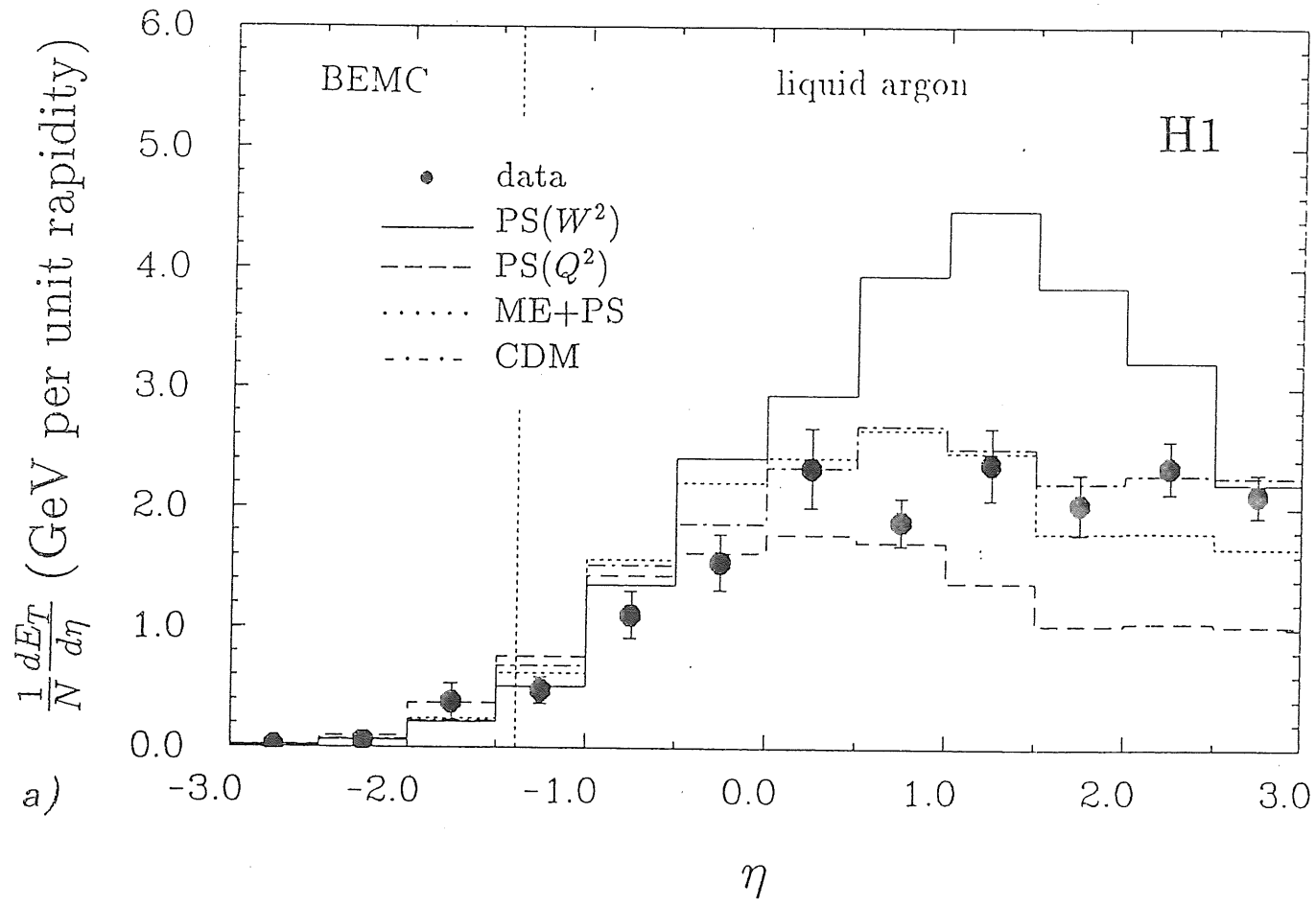
BEMC
liquid argon
H1
data
PS(W^2)
PS(Q^2)
ME+PS
CDM
$\frac{1}{N}\frac{dE_T}{d\eta}$ (GeV per unit rapidity)
η
a)

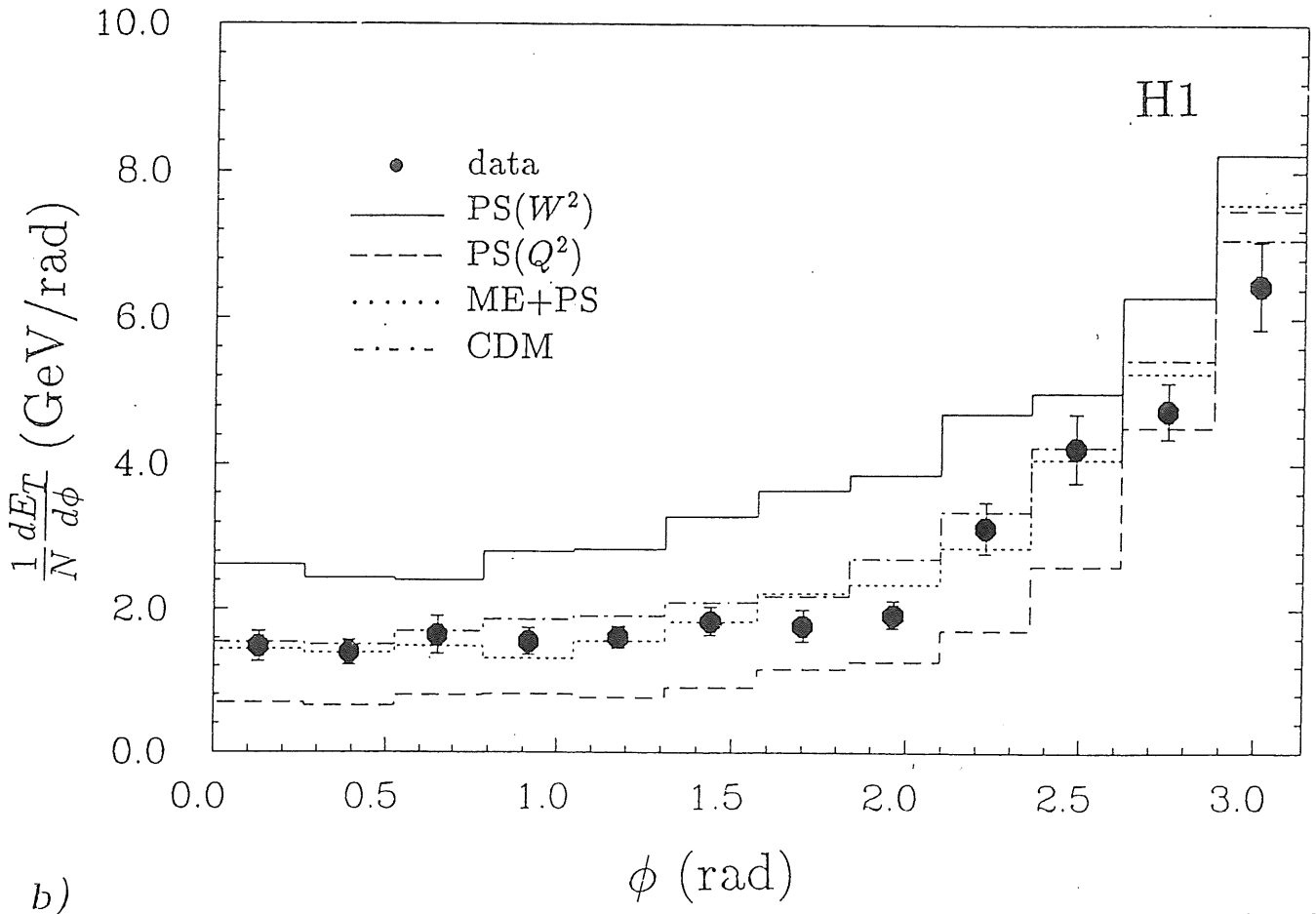
H1
data
PS(W^2)
PS(Q^2)
ME+PS
CDM
$\frac{1}{N}\frac{dE_T}{d\phi}$ (GeV/rad)
ϕ (rad)
b)

Fig. 3

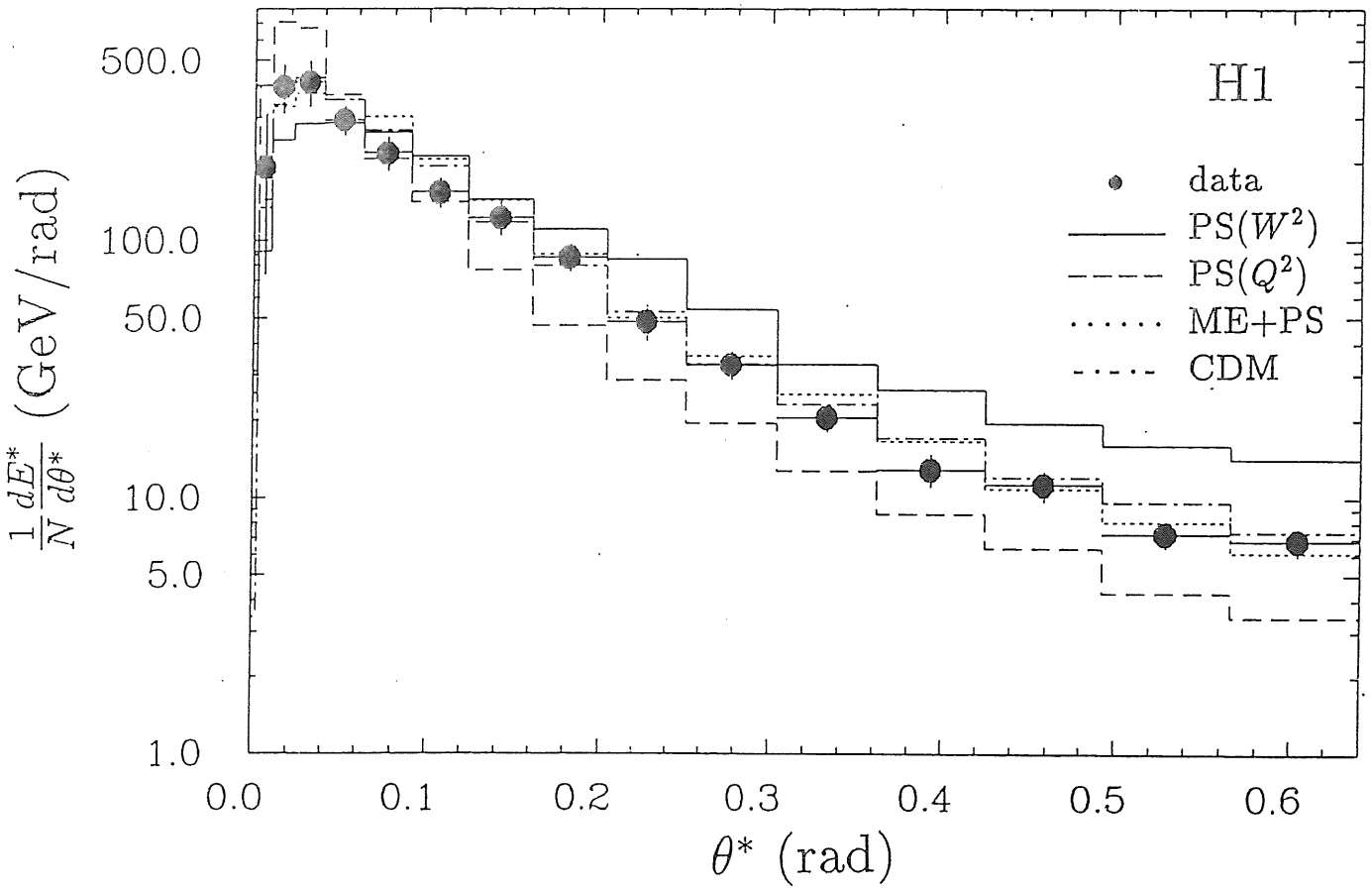
H1
data
PS(W^2)
PS(Q^2)
ME+PS
CDM
500.0
100.0
50.0
10.0
5.0
1.0
0.0
0.1
0.2
0.3
0.4
0.5
0.6
$\frac{1}{N}\frac{dE^*}{d\theta^*}$ (GeV/rad)
θ^* (rad)

Fig. 4

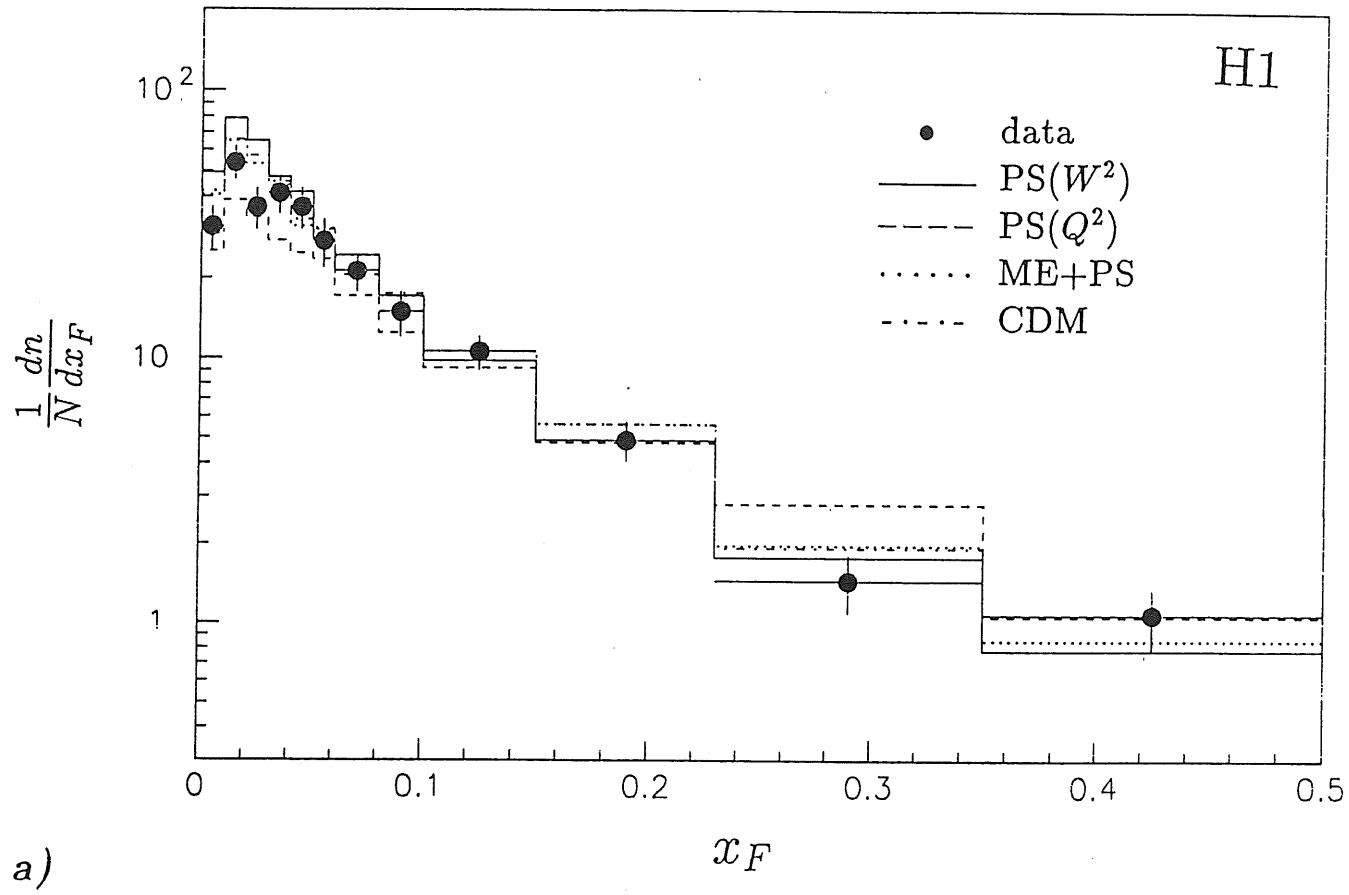
H1
data
PS(W^2)
PS(Q^2)
ME+PS
CDM
$\frac{1}{N}\frac{dn}{dx_F}$
10^2
10
1
0
0.1
0.2
0.3
0.4
0.5
x_F

a)

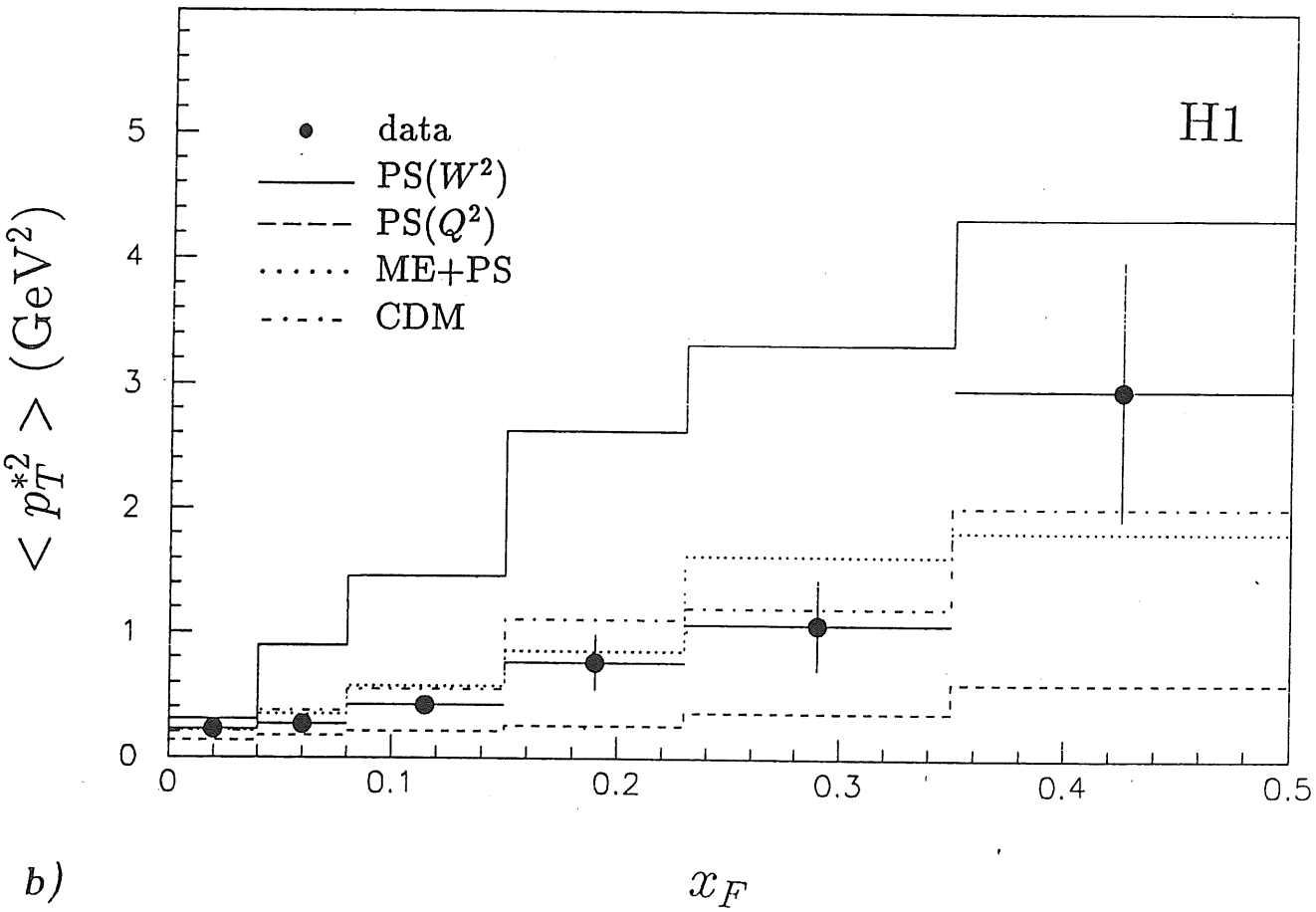
H1
data
PS(W^2)
PS(Q^2)
ME+PS
CDM
$< p_T^{*2} >$ (GeV^2)
5
4
3
2
1
0
0
0.1
0.2
0.3
0.4
0.5
x_F

b)

Fig. 5